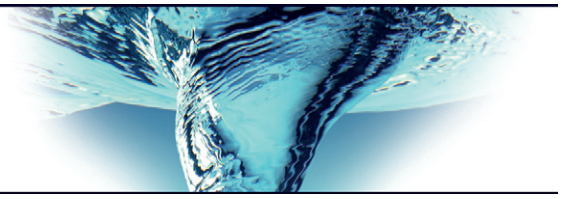
CrossMark

J. Fluid Mech. (2017), *vol.* 812, R2, doi:10.1017/jfm.2016.836



JFM RAPIDS
journals.cambridge.org/rapids

Liquid rope coiling: a synoptic view

Neil M. Ribe†

Laboratoire FAST, Univ. Paris-Sud, CNRS, Univ. Paris-Saclay, 23-25 rue Jean Rostand, Parc Club Orsay Université, F-91405 Orsay, France

(Received 19 October 2016; revised 6 December 2016; accepted 6 December 2016; first published online 28 December 2016)

In liquid rope coiling, a slender jet of viscous fluid falling onto a rigid surface builds a rotating corkscrew-like structure. Here, I use a numerical continuation method to construct a complete regime diagram for liquid rope coiling. I first consider the onset of coiling, and show that a suitable onset criterion is that the radius a_1 of the rope itself be just equal to the radius R of the coil. Numerical calculation of the critical surface $a_1 = R$ in the space of the dimensionless fall height Π_H, flow rate Π_Q and nozzle diameter Π_d shows that the surface has four distinct asymptotic limits corresponding to a viscous (V) mode, a gravitational (G) mode and two inertial modes (I1, I2) which are distinguished by how much the tail of the jet is stretched by gravity. Exact expressions for the onset frequencies in each of these four modes are determined. Finally, the regime diagram is constructed in the form of contour plots of the dimensionless coiling frequency as a function of Π_H and Π_Q for several values of Π_d. The diagram exhibits a total of six modes: V, G, I1, I2, a multivalued inertio-gravitational (IG) mode and a third inertial mode I3 with viscosity-dominated stretching of the tail. The regime diagram permits prediction of the coiling frequency for given values of the fall height, flow rate, viscosity and nozzle diameter, and should therefore be useful in practical applications ranging from non-woven textile production to 3D printing.

Key words: interfacial flows (free surface), jets

1. Introduction

Free liquid jets offer some of the most fascinating and beautiful phenomena in fluid mechanics. Probably the most familiar of these is the 'liquid rope-coil' effect (Barnes & Woodcock 1958) which occurs when a thin stream of honey falls onto a piece of toast. If the fall height is large enough, the falling stream builds a whirling corkscrew-like structure which resembles a pile of coiled rope played out by a mountaineer. Liquid rope coiling has been extensively studied, using laboratory experiments (Barnes & Woodcock 1958; Barnes & MacKenzie 1959;

† Email address for correspondence: ribe@fast.u-psud.fr

© Cambridge University Press 2016

https://doi.org/10.1017/jfm.2016.836 Published online by Cambridge University Press

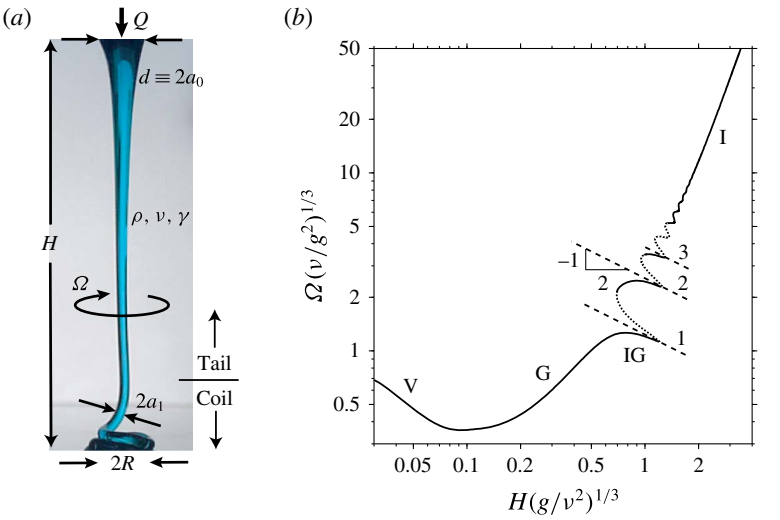


FIGURE 1. (*a*) Parameters of a typical laboratory setup used to study liquid rope coiling. Fluid with density ρ, kinematic viscosity ν and coefficient of surface tension γ is ejected at a volumetric rate Q from a nozzle of diameter d and falls a distance H onto a rigid surface, where it forms a coil of radius R. The radius of the rope in the coil is a_1, and the angular frequency of coiling is Ω. (*b*) Coiling frequency as a function of height, calculated numerically for $d(g/\nu Q)^{1/4} = 0.272$ and $Q(g/\nu^5)^{1/3} = 3.78 \times 10^{-7}$. The dotted portions of the curve are unstable to small perturbations (Ribe *et al.* 2006*a*). The dashed lines show the frequencies of the first three pendulum modes of the tail. The labels V, G, IG and I indicate the portions of the curve corresponding to the viscous, gravitational, inertio-gravitational and inertial modes respectively.

Cruickshank 1980; Cruickshank & Munson 1981; Huppert 1986; Griffiths & Turner 1988; Mahadevan, Ryu & Samuel 1998; Maleki *et al.* 2004; Habibi *et al.* 2006, 2010, 2014; Ribe *et al.* 2006*b*; Ribe, Habibi & Bonn 2006*a*), linear stability analysis (Cruickshank 1988; Tchavdarov, Yarin & Radev 1993; Ribe *et al.* 2006*a*), scaling analysis (Mahadevan, Ryu & Samuel 2000), asymptotic analysis (Blount 2010) and numerical analysis based on slender-rope theory (Maleki *et al.* 2004; Ribe 2004; Habibi *et al.* 2006, 2010, 2014; Ribe *et al.* 2006*b*,*a*).

The main result of the aforementioned studies is that liquid rope coiling can occur in four different modes – viscous, gravitational, inertio-gravitational and inertial – depending on how the viscous forces that resist the bending of the rope are balanced. In the viscous (V) mode, both gravity and inertia are negligible, and the coiling is like that of toothpaste squeezed slowly from a tube onto a nearby surface. In the gravitational (G) mode, the viscous forces that resist bending are balanced by gravity. In the inertio-gravitational (IG) mode, the long 'tail' of the rope behaves like a distributed pendulum, entering into resonance with the coil when the frequency fixed by the latter is close to one of the natural frequencies of the tail. Finally, in the inertial (I) mode, the viscous forces are balanced by inertia in the coil.

In the laboratory, the principal control parameter that determines which mode obtains is the fall height H, which is typically varied while the fluid properties and the flow rate are held constant. Figure 1(*a*) shows the principal geometric and physical parameters of a typical laboratory set-up. Figure 1(*b*) displays a numerically

https://doi.org/10.1017/jfm.2016.836 Published online by Cambridge University Press

calculated curve of coiling frequency versus height, which shows that the coiling modes appear in the order V–G–IG–I as the fall height increases.

The previous studies cited above have given us a remarkably detailed understanding of each of these four modes. However, what is still lacking is a complete regime diagram of the modes as a function of the parameters that control the coiling frequency: the fall height H, the fluid viscosity ν, the volumetric flow rate Q and the nozzle diameter d. Our situation at present is like that of the proverbial blind men exploring the elephant: we have a deep understanding of each of the beast's individual parts, and our task now is to synthesize them into a synoptic portrait of the whole.

2. Dimensional analysis

If the minor effect of surface tension is neglected, the coiling frequency Ω depends on H, Q, ν, d and the gravitational acceleration g. Of these six parameters, two have independent dimensions. Buckingham's Π-theorem then states that there are four independent dimensionless groups, which I take to be

$$\Pi_\Omega = \Omega\left(\frac{\nu}{g^2}\right)^{1/3}, \quad \Pi_H = H\left(\frac{g}{\nu^2}\right)^{1/3}, \quad \Pi_Q = Q\left(\frac{g}{\nu^5}\right)^{1/3}, \quad \Pi_d = d\left(\frac{g}{\nu Q}\right)^{1/4}. \tag{2.1a–d}$$

The parameter Π_d is the ratio of the nozzle diameter d to the length scale

$$\delta = \left(\frac{\nu Q}{g}\right)^{1/4}, \tag{2.2}$$

which is of the order of the arcwise extent of the bending boundary layer in gravitational coiling (Ribe *et al.* 2006*b*). The dimensionless frequency obeys a law of the form

$$\Pi_\Omega = \mathrm{fct}\left(\Pi_H, \Pi_Q, \Pi_d\right). \tag{2.3}$$

The above relationship can be represented by contour plots of Π_Ω as a function of Π_H and Π_Q for several values of Π_d. The ensemble of these plots will be the basis for the regime diagram that is sought.

3. Onset of coiling

The path to a regime diagram naturally starts with a consideration of the onset of coiling. The traditional way to determine the coiling onset criterion is to perform a linear stability analysis of a steady axisymmetric stagnation flow of a fluid jet falling from a nozzle onto a plate some distance below (Tchavdarov *et al.* 1993). However, the stagnation flow can only be steady if the plate is permeable, and if it is not then the jet must be infinitely wide at the bottom. This serious drawback of the linear stability approach means that we need to seek an alternative criterion for the onset of coiling.

A simple geometrical criterion arises from the fact that there are two distinct length scales in the coil: the radius R of the coil and the radius a_1 of the rope itself. Now, coiling can only occur if $R \geqslant a_1$; otherwise, the rope would intersect itself in the centre of the coil. Accordingly, Habibi *et al.* (2014) proposed that $a_1 = R$ is the critical condition for the onset of coiling. Since the numerical continuation method of Ribe (2004) predicts both R and a_1, it can be used to determine the critical surface as a

https://doi.org/10.1017/jfm.2016.836 Published online by Cambridge University Press

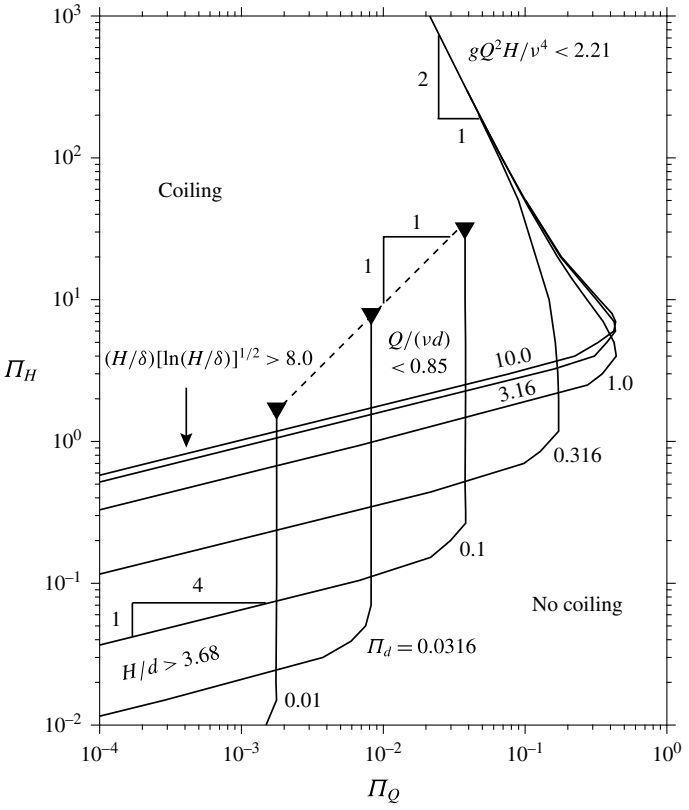


FIGURE 2. Existence of steady coiling solutions, determined numerically using the method of Ribe (2004). Each curve is a locus of points where $a_1 = R$ for a given value of $\Pi_d = d(g/\nu Q)^{1/4} \equiv d/\delta$. Each curve divides the diagram into regions where steady coiling solutions with $a_1 < R$ exist (above and to the left) and do not exist (below and to the right). Black inverted triangles indicate values of Π_H above which critical solutions with $a_1 = R$ do not exist. Inequalities give the criteria for the onset of coiling corresponding to different parts of the diagram.

function of Π_H, Π_Q and Π_d. The procedure is to start with a finite-amplitude coiling solution with $a_1 < R$, and then to continue it numerically until a_1 just equals R.

The result of this procedure is shown in figure 2, which displays critical curves $a_1 = R$ for seven different values of $\Pi_d \in [0.01, 10]$. These curves are in fact cross-sections of a critical surface in the three-dimensional parameter space (Π_H, Π_Q, Π_d). The logarithms of the values of Π_d are evenly spaced to assist in identifying intermediate asymptotic limits, of which four are evident. The first is represented by the line with slope -2 at upper right, where the four curves for $\Pi_d \geqslant 0.316$ coincide. Coiling in this limit occurs when $gQ^2H/\nu^4 < 2.21$, and corresponds to one variety of the inertial (I) mode, as will be explained below. The second limit occurs for low values of $\Pi_d \leqslant 0.1$ for which the upper parts of the critical curves are vertical. Here, coiling occurs when $Q/(\nu d) < 0.85$. The inverted triangles in figure 2 indicate where the critical solutions cease to exist, as evidenced by failure of the numerical algorithm. This limit, which corresponds to a second variety of inertial coiling, has not previously been reported to the best of my knowledge. The third and

https://doi.org/10.1017/jfm.2016.836 Published online by Cambridge University Press

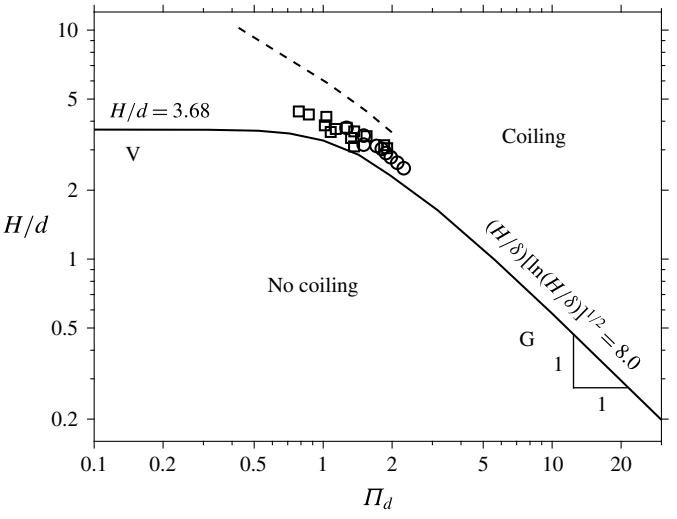


FIGURE 3. Critical curve $a_1 = R$ (solid line) in the inertia-free (Stokes) limit, separating regions where coiling occurs (above) and does not occur (below). The symbols are experimentally measured critical heights (Cruickshank 1980) for silicone oil with $\gamma/\rho g d^2 = 0.0063$ (circles) and 0.014 (squares), corresponding to the limit of small surface tension. The dashed line is the critical curve predicted by the linear stability analysis of Tchavdarov *et al.* (1993) in the absence of surface tension. The asymptotic expressions for the portions of the critical curve corresponding to V and G onset are shown.

fourth limits are in the left portion of the diagram where inertia is negligible. At lower left, the critical curve with slope 1/4 corresponds to the V mode, for which coiling occurs when $H/d > 3.68$. At centre left, the critical curve is that of the G mode, which occurs when $(H/\delta)[\ln(H/\delta)]^{1/2} > 8.0$. The logarithmic factor in the expressions for the radius R and the frequency Ω of gravitational coiling was first found by Blount (2010).

A natural question at this point is whether the critical curves of figure 2 agree with measurements of coiling onset in laboratory experiments. Figure 3 shows the critical curve for the V and G modes, obtained from the leftmost portion of figure 2. The V mode corresponds roughly to $\Pi_d < 0.5$, while the G mode obtains for $\Pi_d > 2$. Also shown in figure 3 are experimental measurements of the critical fall height for the onset of coiling for small values of the inverse Bond number $\gamma/\rho g d^2$, where γ is the coefficient of surface tension (squares and circles; Cruickshank 1980). Finally, the dashed line is the prediction of the critical height for $\gamma = 0$ from the linear stability analysis of Tchavdarov *et al.* (1993). While the experimental measurements do not agree perfectly with the critical curve $a_1 = R$, they are significantly closer to that curve than to the prediction of the linear stability analysis. The most likely reason for the remaining discrepancy is that the rope is fairly thick in the parameter range of the experiments, so that the slender-rope approximation upon which the numerical code is based becomes inaccurate. Nevertheless, it seems reasonable to conclude from figure 3 that $a_1 = R$ is an appropriate criterion for the onset of coiling observed in laboratory experiments. In what follows, I shall study numerically how the coiling frequency depends on the dimensionless parameters Π_H, Π_Q and Π_d.

https://doi.org/10.1017/jfm.2016.836 Published online by Cambridge University Press

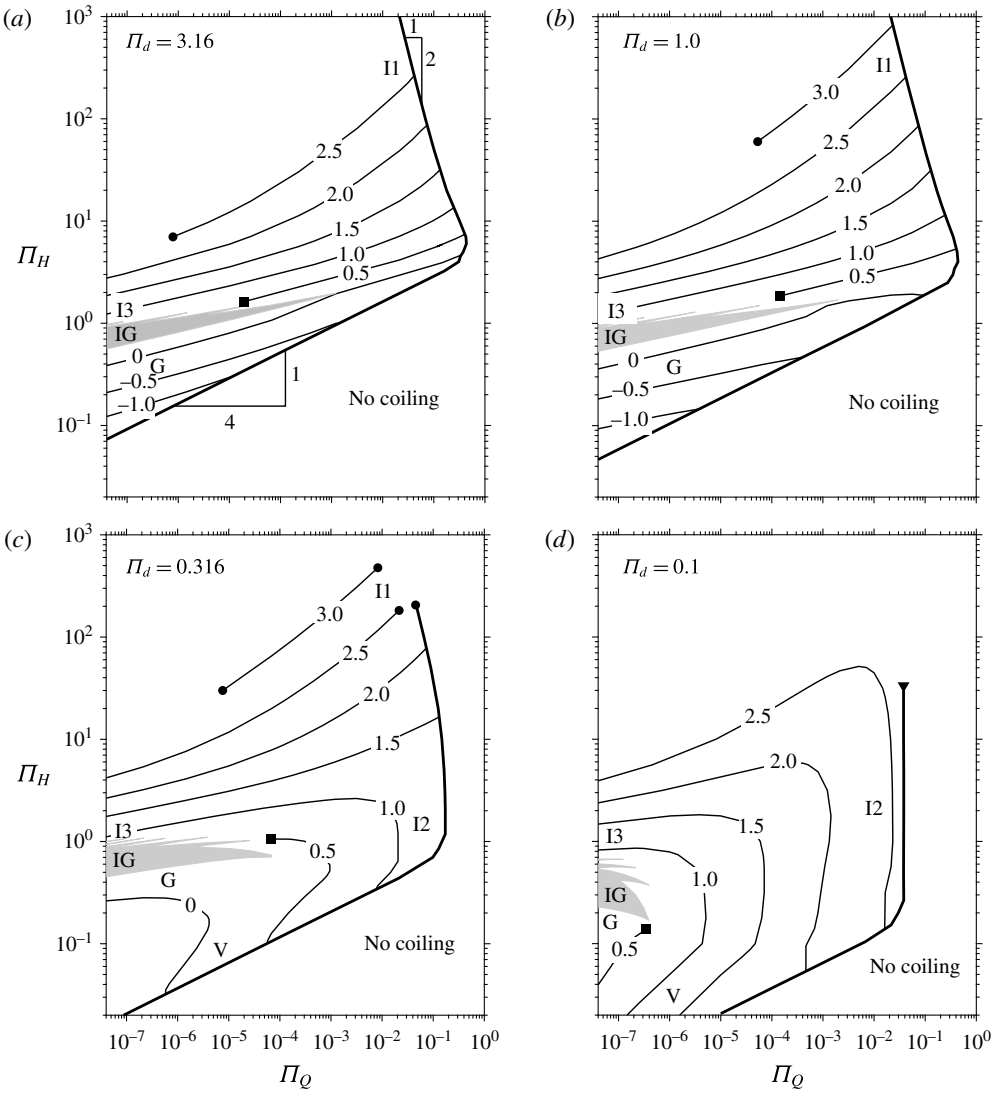


FIGURE 4. Contour plots of the dimensionless coiling frequency Π_Ω as a function of Π_Q and Π_H for four values of Π_d, determined numerically using the method of Ribe (2004). The labels on the contours are $\log_{10}\Pi_\Omega$. Black circles indicate where convergence of the numerical algorithm failed, and black squares show where the calculation was stopped deliberately to avoid entering the multivalued regions (grey). The heavy black lines are the critical curves for coiling onset from figure 2. The labels V, G, IG, I1, I2 and I3 indicate roughly where the corresponding coiling modes reside in the regime diagram.

4. Coiling frequency

The frequency of steady coiling can be predicted using the numerical method of Ribe (2004) for any values of Π_H and Π_Q that lie above and to the left of the critical curves of figure 2. Figure 4 shows contour plots of the dimensionless coiling frequency Π_Ω for four values of Π_d. The heavy line on each plot is the critical curve

https://doi.org/10.1017/jfm.2016.836 Published online by Cambridge University Press

for coiling onset from figure 2. To make the connection with figure 1(*b*), note that the curve in that figure (for which $\Pi_d = 0.272$) is very similar to a vertical slice at $\Pi_Q = 3.78 \times 10^{-7}$ through figure 4(*c*) (for which $\Pi_d = 0.316$). In figures 4(*c*) and 4(*d*), the contours at lower left loop back on themselves, indicating that the frequency passes through a minimum as the fall height H is increased. This behaviour, which is also evident in figure 1(*b*), corresponds to the transition from V coiling (for which $\mathrm{d}\Omega/\mathrm{d}H < 0$) to G coiling (for which $\mathrm{d}\Omega/\mathrm{d}H > 0$). The grey regions in figure 4 correspond to the multivalued IG mode. A typical variation of Ω as a function of H for the IG mode is the portion $\Pi_H \in [0.7, 1.6]$ of the curve in figure 1(*b*).

I begin by determining the coiling onset frequency for the four intermediate asymptotic limits of the critical curves indicated in figure 2. As a preliminary, I note that the frequency of inertial coiling has three distinct scaling laws, depending on the magnitude of the gravitational stretching of the tail. All are based on the fundamental scaling law for the frequency of inertial coiling, which is (Mahadevan *et al.* 2000)

$$\Omega_I \sim \left(\frac{Q^4}{\nu a_1^{10}}\right)^{1/3}. \tag{4.1}$$

In the first inertial mode, which I call I1, the tail is in free fall and the viscous resistance to stretching is negligible. In this case, the radius $a_1 \sim (Q^2/gH)^{1/4}$, whence (4.1) becomes

$$\Omega_I^{(1)} \sim \left(\frac{g^5}{\nu^2 Q^2}\right)^{1/6} H^{5/6}. \tag{4.2}$$

A second inertial mode (I2) has negligible stretching in the tail, so that $a_1 \approx d/2$. The scaling law for this mode is therefore

$$\Omega_I^{(2)} \sim \left(\frac{Q^4}{\nu d^{10}}\right)^{1/3}. \tag{4.3}$$

Finally, in the third inertial mode (I3), the tail is strongly stretched by gravity, but the latter is balanced by the viscous resistance to stretching rather than by inertia. In this case, $a_1 \sim (\nu Q/gH^2)^{1/2}$, and (4.1) becomes

$$\Omega_I^{(3)} \sim \left(\frac{g^5}{\nu^6 Q}\right)^{1/3} H^{10/3}. \tag{4.4}$$

As we shall see, these three inertial modes blend smoothly into one another on the regime diagram.

Figure 5 shows the dimensionless coiling frequency Π_Ω on the critical surface as a function of relevant dimensionless parameters for the four onset modes V (*a*), G (*b*), I1 (*c*) and I2 (*d*). The dimensional equation for the best-fitting regression line is shown on each panel. As an illustration of how the onset frequency may be written in a more familiar form, consider the mode I1, for which the best-fitting regression line is (in dimensional form)

$$\Omega = 1.21 Hg/\nu. \tag{4.5}$$

By using the definition $gQ^2H/\nu^4 = 2.21$ of the critical surface for this mode, one can rewrite the right-hand side of (4.5) by multiplying it by the unitary quantity $(2.21\nu^4/gQ^2H)^{1/6}$, whence

$$\Omega = 1.21\frac{Hg}{\nu}\left(\frac{2.21\nu^4}{gQ^2H}\right)^{1/6} = 1.38\left(\frac{g^5}{\nu^2 Q^2}\right)^{1/6} H^{5/6}. \tag{4.6}$$

https://doi.org/10.1017/jfm.2016.836 Published online by Cambridge University Press

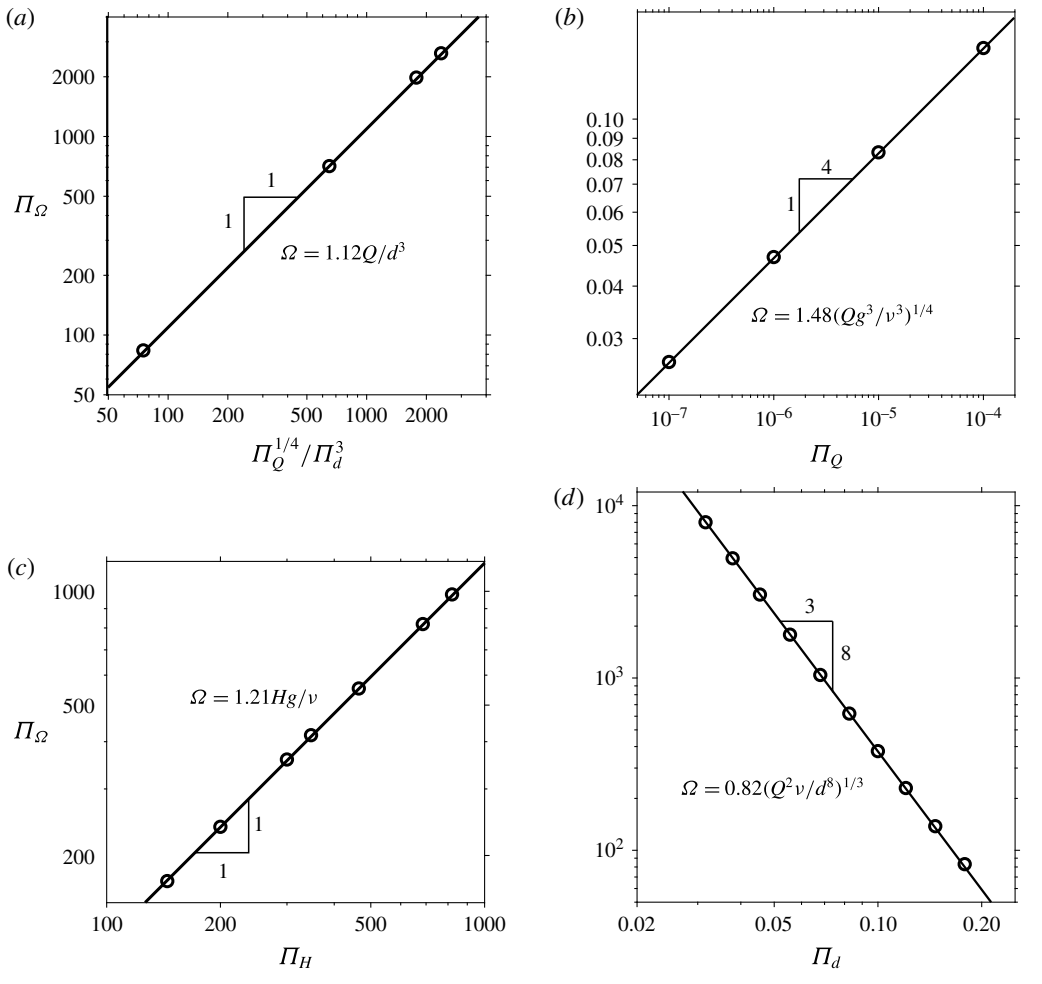


FIGURE 5. Dimensionless coiling frequency Π_Ω on the critical surface as a function of relevant dimensionless parameters for the four onset modes (*a*) V, (*b*) G, (*c*) I1 and (*d*) I2. The dimensional form of the best-fitting regression line is indicated on each panel.

Comparison of (4.6) with (4.2) shows that the onset of coiling along the portion of the critical curve defined by $gQ^2H/\nu^4 = 2.21$ does indeed correspond to the I1 mode of inertial coiling.

A similar analysis applied to the remaining three intermediate asymptotic limits in figure 2 yields scaling laws for the onset frequency for the three additional modes V, G and I2. The results for all four modes are summarized in table 1. The auxiliary conditions in the third column specify where in the parameter space Π_H–Π_Q–Π_d each of the onset criteria applies.

With the above results in hand, it is now possible to construct a complete regime diagram for liquid rope coiling. This diagram is just the set of four contour plots of figure 4, with the coiling modes corresponding to the different regions now indicated. The desired synoptic portrait of the 'whole elephant' is thus complete.

https://doi.org/10.1017/jfm.2016.836 Published online by Cambridge University Press

Mode	Onset criterion	Auxiliary conditions	Onset frequency
V	$H/d > 3.68$	$\Pi_d \ll 1,\ \Pi_Q \ll \Pi_H$	$4.10Q/(d^2H)$
G	$(H/\delta)[\ln(H/\delta)]^{1/2} > 8.0$	$\Pi_d \gg 1,\ \Pi_H \leqslant \Pi_d\Pi_Q^{1/4}$	$0.055H^2(g^5/\nu^5Q)^{1/4}[\ln(H/\delta)]^{-1/2}$
I1	$gQ^2H/\nu^4 < 2.21$	$\Pi_d \geqslant 0.32,\ \Pi_H \geqslant 100$	$1.38(g^5/\nu^2Q^2)^{1/6}H^{5/6}$
I2	$Q/\nu d < 0.85$	$\Pi_d \ll 1,\ 7.0 \leqslant \Pi_H\Pi_Q^{-1} \leqslant 900$	$0.91\ (Q^4/\nu d^{10})^{1/3}$

TABLE 1. Onset of coiling: asymptotic limits.

5. Discussion

Perhaps surprisingly for a phenomenon that has been so extensively studied, the complete regime diagram for liquid rope coiling has not been determined until now. In this study, the regime diagram was constructed as a set of contour plots of the dimensionless coiling frequency Π_Ω as a function of the dimensionless fall height Π_H and flow rate Π_Q for several values of the dimensionless nozzle diameter Π_d. The ensemble of these plots allows the coiling frequency to be predicted as a function of the fall height H, the flow rate Q, the viscosity ν and the nozzle diameter d. The regime diagram should therefore be of interest to researchers working with liquid rope coiling in practical situations ranging from fibre laydown in non-woven textile production to 3D printing.

An interesting feature of the regime diagram is the presence of three distinct varieties of the inertial mode, which differ according to the amount of gravitational stretching in the tail. In particular, that stretching is negligible in mode I2, and the corresponding portion of the regime diagram is here identified for the first time. The mode I3 differs from I1 and I2 in that it is not an onset mode, but only exists in the interior of the regime diagram, well away from the critical onset surface. The same is true of the multivalued IG mode.

The work presented here corrects a small error in Habibi *et al.* (2010), who proposed onset criteria (but not onset frequencies) for the three modes V, G and I1. Instead of the correct onset criterion $a_1 = R$, these authors determined the locus of points where the numerical solutions exhibit a turning point or fold as the ratio a_1/R increases. Because the jet is parameterized by arclength, there is nothing to prevent it from intersecting itself numerically, and indeed it is found that steady solutions can exist up to approximately $a_1/R = 1.95$ before the turning point is reached. Use of the (mistaken) turning point criterion changes the numerical factors in table 1 by only approximately 5 %–6 %, but nevertheless the correct values determined in the present study should be used.

Turning towards the future, I believe that the principal remaining task is to understand the inertio-gravitational (IG) coiling mode in greater depth. In this mode, the tail of the rope acts as a distributed pendulum which is forced at the bottom by the bending stresses applied by the coil. The tail enters into resonance with the coil when one of its natural frequencies is close to the frequency fixed by the coil. This is manifested in the downward/rightward facing peaks in the curve of frequency versus fall height in figure 1(*b*), which are classic resonance peaks whose amplitudes are limited by the nonlinear effects of inertia (Ribe *et al.* 2006*b*). I understand that two colleagues are currently carrying out an analytical study of this complicated behaviour, and I look forward eagerly to their results.

https://doi.org/10.1017/jfm.2016.836 Published online by Cambridge University Press

Acknowledgements

This research was supported in part by a grant from the SEDIT program of the institute INSU of the CNRS. I thank three anonymous referees for constructive comments which helped to improve the original paper.

References

BARNES, G. & MACKENZIE, R. 1959 Height of fall versus frequency in liquid rope-coil effect. *Am. J. Phys.* **27**, 112–115.

BARNES, G. & WOODCOCK, R. 1958 Liquid rope-coil effect. *Am. J. Phys.* **26**, 205–209.

BLOUNT, M. 2010 Bending and buckling of a falling viscous thread. PhD thesis, University of Cambridge, Cambridge, UK.

CRUICKSHANK, J. O. 1980 Viscous fluid buckling: a theoretical and experimental analysis with extensions to general fluid stability. PhD thesis, Iowa State University, Ames, Iowa.

CRUICKSHANK, J. O. 1988 Low-Reynolds-number instabilities in stagnating jet flows. *J. Fluid Mech.* **193**, 111–127.

CRUICKSHANK, J. O. & MUNSON, B. R. 1981 Viscous fluid buckling of plane and axisymmetric jets. *J. Fluid Mech.* **113**, 221–239.

GRIFFITHS, R. W. & TURNER, J. S. 1988 Folding of viscous plumes impinging on a density or viscosity interface. *Geophys. J.* **95**, 397–419.

HABIBI, M., HOSSEINI, S. H., KHATAMI, M. H. & RIBE, N. M. 2014 Liquid supercoiling. *Phys. Fluids* **26**, 024101.

HABIBI, M., MALEKI, M., GOLESTANIAN, R., RIBE, N. M. & BONN, D. 2006 Dynamics of liquid rope coiling. *Phys. Rev.* E **74**, 066306.

HABIBI, M., RAHMANI, Y., BONN, D. & RIBE, N. M. 2010 Buckling of liquid columns. *Phys. Rev. Lett.* **104**, 074301.

HUPPERT, H. E. 1986 The intrusion of fluid mechanics into geology. *J. Fluid Mech.* **173**, 557–594.

MAHADEVAN, L., RYU, W. S. & SAMUEL, A. D. T. 1998 Fluid 'rope trick' investigated. *Nature* **392**, 140.

MAHADEVAN, L., RYU, W. S. & SAMUEL, A. D. T. 2000 Correction: fluid 'rope trick' investigated. *Nature* **403**, 502.

MALEKI, M., HABIBI, M., GOLESTANIAN, R., RIBE, N. M. & BONN, D. 2004 Liquid rope coiling on a solid surface. *Phys. Rev. Lett.* **93**, 214502.

RIBE, N. M. 2004 Coiling of viscous jets. *Proc. R. Soc. Lond.* A **460**, 3223–3239.

RIBE, N. M., HABIBI, M. & BONN, D. 2006*a* Stability of liquid rope coiling. *Phys. Fluids* **18**, 084102.

RIBE, N. M., HUPPERT, H. E., HALLWORTH, M. A., HABIBI, M. & BONN, D. 2006*b* Multiple coexisting states of liquid rope coiling. *J. Fluid Mech.* **555**, 275–297.

TCHAVDAROV, B., YARIN, A. L. & RADEV, S. 1993 Buckling of thin liquid jets. *J. Fluid Mech.* **253**, 593–615.

https://doi.org/10.1017/jfm.2016.836 Published online by Cambridge University Press